



Population imaging of enterochromaffin cell activity reveals regulation by somatostatin

Nathan D. Rossen^{ab} , Kouki K. Touhara^a, Joel Castro^{cd}, Andrea M. Harrington^{cd}, Sonia Garcia Caraballo^{cd}, Fei Deng^{ef}, Yulong Li^{ef} , Stuart M. Brierley^{cd}, and David Julius^{a,1}

Affiliations are included on p. 9.

Contributed by David Julius; received January 21, 2025; accepted April 7, 2025; reviewed by Arthur Beyder and Michael A. Fischbach

Sensory enteroendocrine cells in the intestinal epithelium detect and relay information about the luminal environment to other cells within and outside the gut. Serotonergic enterochromaffin (EC) cells are a subset of enteroendocrine cells that detect noxious stimuli within the gut lumen, such as chemical irritants and microbial byproducts, and transduce this information to sensory nerve fibers to elicit defensive responses such as nausea and visceral pain. While much has recently been learned about the pharmacological and biophysical characteristics of EC cells, a more broadscale investigation of their properties has been hindered by their relatively low prevalence and sparse anatomical distribution within the gut epithelium. Here, we introduce a method for large-scale parallel analysis of individual EC cell activity within a physiologically relevant epithelial context. Using this approach, we identify somatostatin-28 as a potent inhibitor of both basal and stimulus-evoked serotonin release from EC cells and delineate the signaling pathway that underlies this modulatory response. Our analysis suggests that targeting this inhibitory signaling pathway may offer therapeutic avenues for treating gastrointestinal disorders associated with EC cell function and dysregulated serotonin signaling. Together with the ongoing development of specific biosensors, this platform provides a template for the efficient characterization of other rare sensory cell types and their pharmacological modulators.

sensory physiology | enterochromaffin cells | somatostatin | biosensors | interoception

The gastrointestinal (GI) tract is continuously exposed to a diverse chemical milieu of nutrients, environmental toxins, and microbial byproducts. Upon entry to the intestine, these chemicals can be directly sensed by epithelial enteroendocrine cells, which express a host of receptors for environmental and endogenous stimuli and secrete neurotransmitters and peptide hormones to relay this information to other cells in the gut and throughout the body (1). Enterochromaffin (EC) cells are a subclass of excitable enteroendocrine cells that release serotonin in response to bacterial metabolites (2), neurotransmitters, peptide hormones (3), interleukins (4), mechanical force (5), and ingested or endogenous irritants (6) thereby modulating GI motility (7), nausea (8), and visceral pain (9). Serotonin receptors expressed within the gut (10) have been targeted pharmacologically to treat intestinal dysmotility and visceral pain associated with irritable bowel syndrome (IBS) (11). Considering that EC cell activity is sufficient to induce acute and persistent visceral hypersensitivity (9), tools to directly inhibit EC cell activity would seem clinically attractive. However, such strategies are not available, motivating the investigation of endogenous mechanisms that regulate EC cell function with the potential to be exploited therapeutically.

The paucity and broad distribution of EC cells across the intestinal epithelium has long complicated their physiological characterization (12). Initial efforts relied on measurements of bulk serotonin outflow from intestinal tissue preparations using chromatographic (13) or immunosorbent (14) assays with relatively low sensitivity or temporal resolution. More recently, advances in mouse genetics and organoid culture have permitted the rigorous biophysical interrogation of these excitable cells using methods such as patch-clamp electrophysiology and calcium imaging (2, 15). While such single-cell assays are sensitive and dynamic, their low throughput in this context makes screening for potential modulators slow and laborious.

To close this technical gap, we have taken advantage of G protein-coupled receptor (GPCR)-based fluorescent biosensors, which have emerged as powerful tools to study neurotransmitter dynamics in vivo and in vitro (16, 17). Here, we demonstrate that biosensor-expressing epithelial monolayers can be exploited as an efficient system for large-scale parallel analysis of low-abundance secretory cells with single-cell resolution.

Significance

Serotonergic enterochromaffin (EC) cells are sensory cells within the gut that detect noxious stimuli and transduce this information to sensory nerve fibers to elicit defensive responses such as nausea and visceral pain. EC cells have been implicated in gastrointestinal disorders such as irritable bowel syndrome, yet they are challenging to study due to their low abundance and sparse distribution. To overcome this hurdle, we developed a fluorescent biosensor-based strategy for the large-scale analysis of EC cell activity and used this method to delineate an inhibitory pathway with therapeutic potential. This technique will likely be useful for future identification of EC cell modulators and may be adapted to the study of other secretory cells in the intestinal epithelium.

Author contributions: N.D.R., K.K.T., S.M.B., and D.J. designed research; N.D.R., K.K.T., J.C., A.M.H., and S.G.C. performed research; N.D.R., F.D., and Y.L. contributed new reagents/analytic tools; N.D.R., J.C., A.M.H., S.G.C., S.M.B., and D.J. analyzed data; and N.D.R. and D.J. wrote the paper.

Reviewers: A.B., Mayo Clinic Minnesota; and M.A.F., Stanford.

Competing interest statement: D.J. is a member of the SAB for Rapport Therapeutics.

Copyright © 2025 the Author(s). Published by PNAS. This article is distributed under [Creative Commons Attribution-NonCommercial-NoDerivatives License 4.0 \(CC BY-NC-ND\)](https://creativecommons.org/licenses/by-nc-nd/4.0/).

¹To whom correspondence may be addressed. Email: david.julius@ucsf.edu.

This article contains supporting information online at <https://www.pnas.org/lookup/suppl/doi:10.1073/pnas.2501525122/-/DCSupplemental>.

Published May 6, 2025.

Using this method, we identify somatostatin as a robust inhibitor of both tonic and stimulus-evoked EC cell activity, then delineate the signaling pathway that mediates this effect, and examine its relevance to visceral hypersensitivity.

Results

As recently reported (6), the fluorescent serotonin biosensor g5-HT3.0 (*aka* gGRAB_{5-HT3.0}) can be used to sensitively monitor EC cell activity within the gut. This membrane protein, composed of a catalytically inactive metabotropic serotonin receptor fused to circularly permuted enhanced green fluorescent protein (cpEGFP), serves as a molecular switch that reports serotonin binding at its extracellular face (*SI Appendix, Fig. S1A*) (18). Mice that express Cre recombinase under control of the promoter for Villin-1 together with a Cre-dependent allele containing g5-HT3.0 (*Villin^{Cre}; Rosa26^{g5-HT3.0}*) express the biosensor throughout the small intestinal and colonic epithelium (6). We established 3-dimensional (3D) epithelial organoids from the jejunum of these mice, dissociated the 3D organoids into small clumps and single cells, and seeded the cell suspension into 384-well tissue culture plates to prepare 2-dimensional (2D) organoid monolayers of ~40 to 80% confluence (*Fig. 1A*). Consistent with previous reports, EC cells were sparsely distributed throughout the monolayers (19), and we observed that g5-HT3.0 expression persisted in all epithelial cells (*SI Appendix, Fig. S1B*). To record biosensor activity, we replaced the culture media with a minimal imaging media to minimize background fluorescence and performed automated widefield imaging of the monolayers at low (4×) magnification to visualize the entirety of each well at once (*Fig. 1A*).

In our recordings, tonic serotonin release from EC cells could be observed as pulsatile changes in g5-HT3.0 fluorescence that often spread to neighboring epithelial cells, similar to our previous observations in *ex vivo* tissue preparations (*SI Appendix, Fig. S1C and Movie S1*) (6). Individual EC cells exhibited a range of tonic activities (*Fig. 1B–D*). In some cells, single serotonin release events were separated by periods of sustained inactivity, while in other cases EC cells exhibited higher-frequency bursts of activity for several minutes at a time (*Fig. 1D*). Applying thapsigargin at the end of each recording (which evokes robust serotonin release via mobilization of ER-Ca²⁺ stores) allowed us to identify EC cells regardless of their level of tonic activity (*SI Appendix, Fig. S1C and D*). To exploit the signal amplification provided by g5-HT3.0 expressed on neighboring cells, we measured individual EC cell activity as the fluorescence intensity over time within ~100 μm-diameter regions centered around each cell, discarding cells for which these regions overlapped. Enteroid monolayers autonomously assemble into dense, crypt-like loci surrounded by larger, villus-like domains (19) and accordingly, we observed differences in cell density around each EC cell (*SI Appendix, Fig. S1B*). To account for the consequent variation in local g5-HT3.0 expression, we normalized the intensity of each signal to that elicited by a maximally effective concentration of serotonin, which we applied following thapsigargin in each experiment (*SI Appendix, Fig. S1C and D*).

To determine whether this system could be used to examine EC cell responses to physiologically relevant stimuli, we elicited membrane depolarization and Ca²⁺ influx in EC cells by applying allyl isothiocyanate (AITC), a specific agonist of the nonselective TRPA1 ion channel (2, 6, 20). Visualization of AITC-treated wells showed an immediate increase in both the intensity and frequency of serotonin release (*SI Appendix, Fig. S1C and D and Movie S1*). To best represent the range of baseline activity we observed across EC cell populations and the effect of AITC stimulation, we used

the normalized sensor traces to calculate two distinct activity metrics for each cell. We expressed the change in peak local serotonin concentration before and after drug application as the difference in maximum signal intensity ($max_{\text{treatment}} - max_{\text{baseline}}$). Because we could not confidently establish the absolute frequency of serotonin release events for many cells, we instead used signal volatility ($vol = \sum |F_{i+1} - F_i| / [t_{\text{max}} - t_0]$), the mean absolute difference between adjacent time points) to quantify the degree of serotonin fluctuation during each phase of the experiment. We expressed the effect of AITC as the log ratio of volatility ($\ln[vol_{\text{treatment}}/vol_{\text{baseline}}]$) such that positive and negative values represent an increase or decrease in EC cell activity, respectively. Both metrics effectively represented the dose-dependent stimulation by AITC that we observed in these cells (*SI Appendix, Fig. S1E*).

We then used these metrics to assess responses to a panel of candidate EC cell modulators that we had not previously tested (2), focusing on neuropeptides and molecules known to modulate pain and inflammation (*Fig. 1B and C*). We were interested to find that one of the compounds that we screened, somatostatin-28 (SST28), had a substantial inhibitory effect on EC cell activity, completely blocking tonic serotonin release from most cells for the remainder of the recording (*Fig. 1D and Movie S2*). Both of our activity metrics clearly represented this effect, with the change in signal volatility being particularly evident (*Fig. 1B and C*). Of the two functional *Sst* (somatostatin) gene products, SST28 is the predominant peptide secreted by enteroendocrine D cells in the intestinal mucosa, whereas the shorter SST14 is produced throughout the rest of the body (21–25). Both molecules serve as ligands for members of the somatostatin receptor (SSTR) family of GPCRs, which primarily signal through the inhibitory G protein (G_i) pathway (26). Indeed, SST14 has been previously proposed to modulate EC cell activity based on bulk measurements of serotonin in supernatants from intestinal tissues or acutely isolated cell suspensions (13, 14). Given the robust inhibitory responses to SST28 that we observed in g5-HT3.0 monolayers, we set out to characterize the molecular mechanisms underlying this action.

SST28 inhibits tonic, low-level serotonin release from EC cells, but can it also diminish higher-level serotonin release evoked by EC cell excitation? To address this question, we treated EC cells with SST28 prior to activating TRPA1 channels with AITC. We observed a significant diminution of stimulus-evoked serotonin release, and at low concentrations of AITC, pretreatment with SST28 reduced EC cell activity to basal levels (*Fig. 2A and B*). To validate that the inhibitory effects we observed were indeed due to SSTR-mediated G_i signaling, we treated g5-HT3.0 monolayers overnight with pertussis toxin (PTX) to inactivate Gα_i subunits. Indeed, while PTX pretreatment did not affect basal EC cell activity, it did abrogate the inhibitory effect of SST28 (*Fig. 2C and D and SI Appendix, Fig. S2A*).

Notably, in these and previous recordings we observed a small proportion of EC cells in which inhibition by SST28 was preceded by a rapid, transient increase in serotonin release (*SI Appendix, Fig. S2B and C*). Canonically inhibitory SSTR family members have been reported to elicit Ca²⁺ flux and PLC activation either through promiscuous engagement of Gα_q subunits (27) or through PTX-sensitive G_i-Gβγ-PLCβ signaling (28). Confirming the involvement of G_q signaling, pretreatment with the Gα_q subunit inhibitor YM254890 (YM) selectively blocked the excitatory phase while the inhibitory effect of SST28 was preserved (*SI Appendix, Fig. S2C–E*). We observed a subtle decrease in baseline serotonin release in YM-treated cells, suggesting a degree of tonic G_q engagement in EC cells within our organoid monolayers (*SI Appendix, Fig. S2F*). PTX also abolished transient excitation

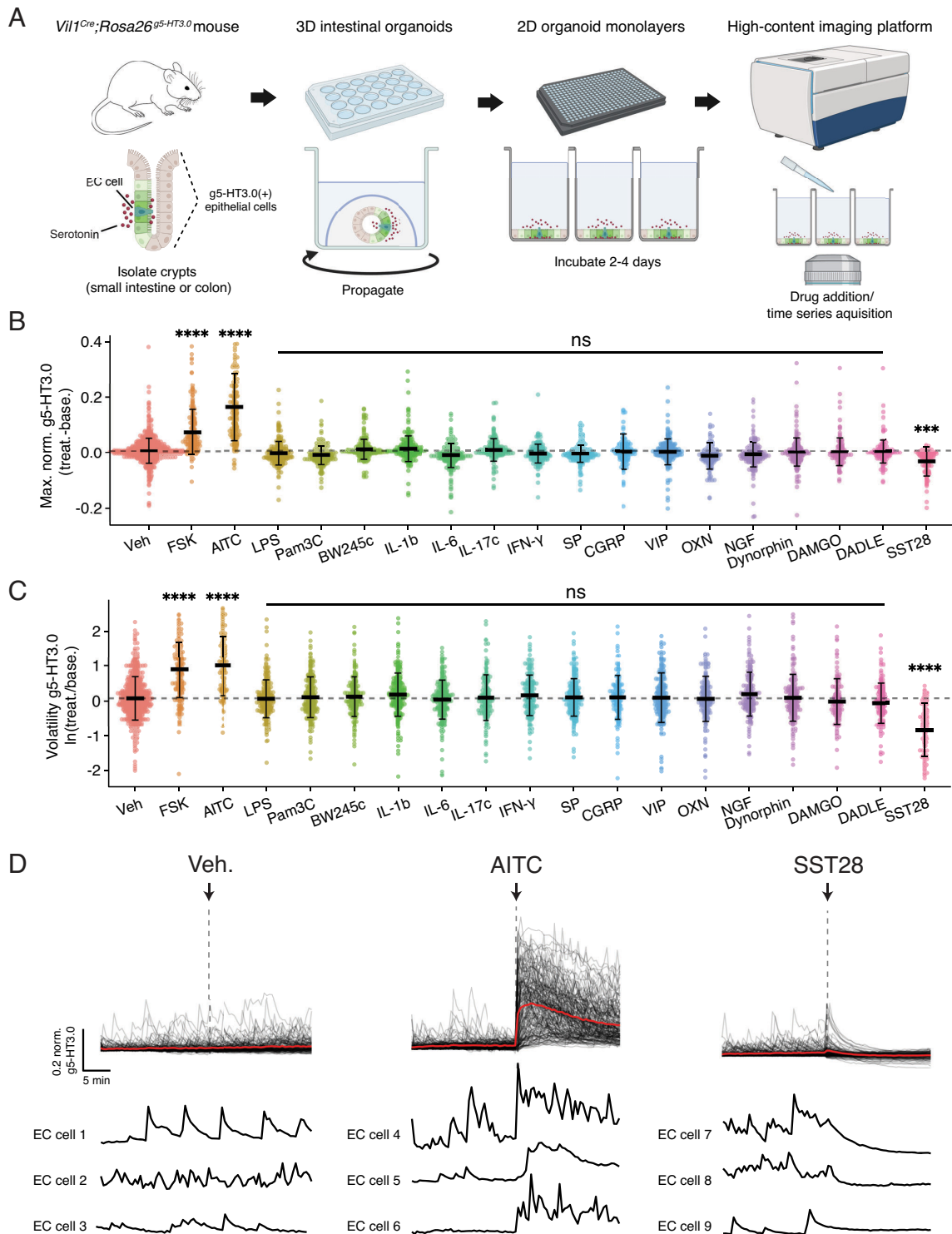


Fig. 1. A chemical screen for EC cell modulators using in vitro serotonin biosensor imaging. (A) 3D epithelial organoids expressing the serotonin sensor g5-HT3.0 were established from the small intestine or colon of *Vil1^{Cre};Rosa26^{g5-HT3.0}* mice. These organoids were used to generate organoid monolayers and EC cell activity was monitored by imaging g5-HT3.0 fluorescence. (B and C) Results from a pharmacological screen of small intestinal EC cells. Plots show the effect of selected compounds on normalized g5-HT3.0 (B) maximum and (C) volatility with each data point representing the response of a single EC cell. Generalized Estimating Equation (GEE) model, *P* values adjusted for multiple comparisons (Bonferroni). All reported *P* values are relative to vehicle (*n* = 704, *N* = 15). FSK (forskolin, 25 μ M, *n* = 186, *N* = 4, max. *P* = 0.0001, vol. *P* < 0.0001), AITC (allyl isothiocyanate, 30 μ M, *n* = 209, *N* = 4, max. *P* = 0.0001, vol. *P* < 0.0001), SST28 (somatostatin-28, 300 nM, *n* = 157, *N* = 4, max. *P* = 0.0001, vol. *P* < 0.0001), DADLE (1 μ M, *n* = 157, *N* = 4, max. *P* > 0.9999, not significant, vol. *P* = 0.6980, not significant). All others (*P* > 0.9999, not significant, vol. *P* > 0.9999, not significant): LPS (lipopolysaccharide, 1 μ M, *n* = 225, *N* = 4), Pam3C (Pam3CSK4, 100 nM, *n* = 221, *N* = 4), BW245c (25 μ M, *n* = 210, *N* = 4), IL-1 β (interleukin 1 β , 50 nM, *n* = 226, *N* = 4), IL-6 (interleukin 6, 100 ng/mL, *n* = 243, *N* = 4), IL-17c (interleukin 17c, 100 ng/mL, *n* = 205, *N* = 4), IFN- γ (interferon γ , 10 nM, *n* = 180, *N* = 3), SP (substance P, 1 μ M, *n* = 236, *N* = 4), CGRP (calcitonin gene-related peptide, 1 μ M, *n* = 181, *N* = 4), VIP (vasoactive intestinal peptide, 300 nM, *n* = 221, *N* = 4), OXN (orexin, 100 nM, *n* = 173, *N* = 4), NGF (nerve growth factor, 100 nM, *n* = 222, *N* = 4), dynorphin (1 μ M, *n* = 192, *N* = 4), DAMGO (1 μ M, *n* = 134, *N* = 3). (D) Representative traces from EC cells treated with vehicle, AITC, or SST28. Vertical lines indicate treatment timepoint. Average trace in red. Isolated traces of EC cells from each condition shown below at the same scale. *n* = number of cells, *N* = number of wells. Error bars: SD. *****P* \leq 0.0001.

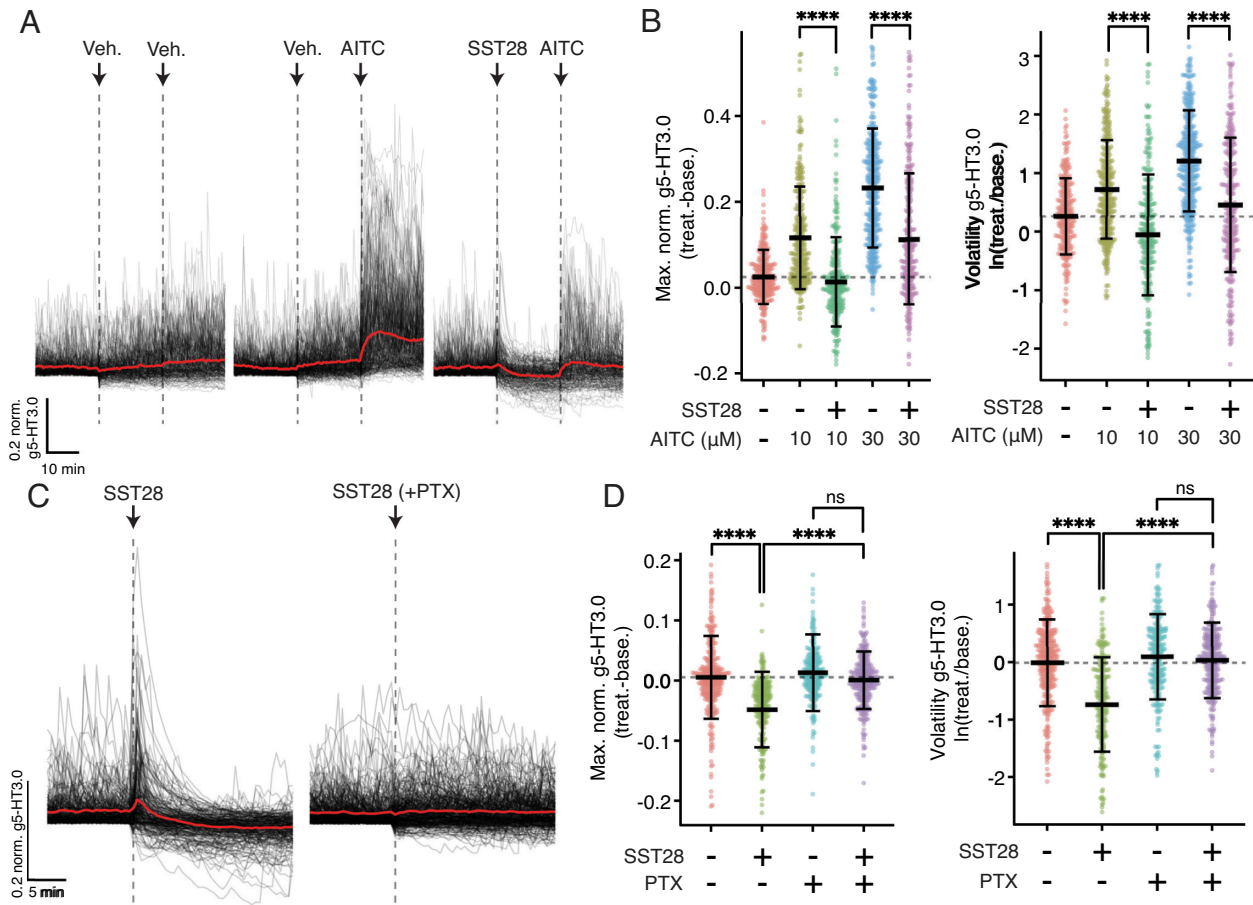


Fig. 2. SST28 inhibits tonic and evoked EC cell activity via G_i signaling. (A) Representative traces showing acute treatment with SST28 (300 nM) inhibiting subsequent EC cell activation by AITC (10 μ M). Vertical lines indicate treatment timepoints. Average trace in red. (B) Effect of SST28 on EC cell activation by AITC. GEE model (Bonferroni). AITC (10 μ M) SST28(-) vs. AITC (10 μ M) SST28(+). (max. $P < 0.0001$, vol. $P < 0.0001$), AITC (30 μ M) SST28(-) vs. AITC (30 μ M) SST28(+). (max. $P < 0.0001$, vol. $P < 0.0001$). AITC- SST28(-) (n = 277, N = 7), AITC (10 μ M) SST28(-) (n = 319, N = 7), AITC (10 μ M) SST28(+). (n = 269, N = 7), AITC (30 μ M) SST28(-) (n = 381, N = 8), AITC (30 μ M) SST28(+). (n = 305, N = 7). (C) Representative traces showing EC cell responses to SST28 (300 nM) blocked by pretreatment with PTX (200 ng/mL) for 24 h. Vertical lines indicate treatment timepoints. Average trace in red. (D) Effect of PTX pretreatment on SST28-evoked changes in g5-HT3.0 maximum and volatility. GEE model (Bonferroni). PTX(-) SST28(-) vs. PTX(-) SST28(+). (max. $P < 0.0001$, vol. $P < 0.0001$), PTX(-) SST28(+). vs. PTX(+). SST28(+). (max. $P < 0.0001$, vol. $P < 0.0001$), PTX(+). SST28(-) vs. PTX(+). SST28(+). (max. $P = 0.26$, not significant, vol. $P > 0.9999$, not significant). PTX(-) SST28(-) (n = 345, N = 17), PTX(-) SST28(+). (n = 236, N = 14), PTX(+). SST28(-) (n = 261, N = 10), PTX(+). SST28(+). (n = 304, N = 13). Data are from three independent experiments. n = number of cells, N = number of wells. Error bars: SD. **** $p \leq 0.0001$.

by SST28 (SI Appendix, Fig. S2C), suggesting that the biphasic responses detectable by g5-HT3.0 imaging resulted from coincident engagement of both G_i and G_q signaling pathways (29).

We were curious to know which of the five SSTR subtypes modulates EC cell activity, and whether this might differ between crypt and villus EC cells. We collected tissue from the small intestine of *Tph1*^{CFP} mice, which specifically express CFP in EC cells (15). We then mechanically separated the crypt and villus epithelia and sorted CFP+ and CFP- cells from the two epithelial fractions (SI Appendix, Fig. S3A). Transcriptional profiles of each of the four populations were obtained using deep (~50 million reads/sample) bulk RNA sequencing to detect differences in low-abundance transcripts such as those encoding GPCRs. As expected, EC cell signature genes were highly expressed in both CFP+ populations relative to other epithelial cells from the same region (SI Appendix, Fig. S3 B–D). In these datasets, we were able to detect expression of four of the five known SSTR subtypes (*Sstr1*, *Sstr2*, *Sstr3*, and *Sstr5*), with *Sstr1* and *Sstr5* being the most highly enriched in both the crypt and villus (Fig. 3A). While specific pharmacological tools for discriminating among SSTR subtypes are rather limited (26, 30) we used the SSTR agonists octreotide (which targets SSTR2, SSTR3, and SSTR5) and CH275 (which is selective for SSTR1) to confirm functional

expression of SSTRs and gain some information about subtype involvement. Octreotide treatment inhibited basal EC cell activity to a similar level as SST28, implicating SSTR2, 3, or 5. Surprisingly, CH275 had no effect on EC cell activity despite the high enrichment of *Sstr1* observed in our sequencing data (Fig. 3 B and C). Several reports have demonstrated functional and transcriptional differences between colon and small intestine EC cells (31–33). To determine whether colon EC cells respond similarly to SSTR agonists compared to those from the small intestine we established colonoid cultures from *Vill1*^{Cre}; *Rosa26*^{g5-HT3.0} mice and prepared monolayers for imaging as described above (Fig. 1A and SI Appendix, Fig. S1B). In colonic EC cells, we observed inhibition by SST28 that was equal, if not greater, than that measured in EC cells from the small intestine (SI Appendix, Fig. S4 A and B). Interestingly, in contrast to the small intestine, the SSTR1 agonist CH275 robustly inhibited tonic activity in colonic EC cells. On the other hand, the effect of octreotide was somewhat reduced in comparison to the pan-receptor agonist SST28. These data suggest that while EC cells in the small intestine primarily express functional SSTR2/3/5, SSTR1 contributes significantly to SST28 responses of these cells in the colon.

To determine whether the responses we observed in organoid monolayers modeled EC cell behavior within the intact crypt-villus

generated jejunal organoids from *Tac1^{Cre};Polr2a^{GCaMP5g-IRES-tdT}* mice, which specifically express GCaMP5g and tdTomato (tdT) in EC cells (6). We then prepared monolayers from these organoids on glass coverslips and visualized GCaMP5g activity under constant perfusion (Fig. 5A). Here, again, we observed tonic, low-level Ca^{2+} flux that was significantly diminished during the application of SST28 (Fig. 5B and C). Furthermore, we found that Ca^{2+} signals elicited by subsaturating concentrations of AITC were also inhibited by SST28 (Fig. 5D–F). Because AITC-evoked serotonin release requires activation of voltage-gated calcium channels (Ca_v) (2), we asked whether SSTR signaling inhibits Ca_v activity in EC cells. In voltage-clamp recordings of primary isolated EC cells from the small intestine of *Tac1^{Cre};Polr2a^{GCaMP5g-IRES-tdT}* mice, Ca_v activity could be observed as depolarization-induced inward currents that were blocked by extracellular Cd^{2+} (Fig. 5G–I). Upon application of octreotide, the amplitude of these currents was rapidly diminished, while the voltage dependence remained unaffected (Fig. 5I–K). We observed a similar degree of inhibition by SST28 (Fig. 5L and M). The effects of SST28 and octreotide were inhibited by PTX, confirming involvement of the G_i signaling pathway (Fig. 5L). Taken together, these data suggest that SSTR-mediated inhibition of serotonin release from EC cells occurs, at least in part, through G_i -mediated suppression of Ca^{2+} influx through voltage-gated calcium channels. In these experiments, we observed robust inhibition of Ca_v currents upon application of the SSTR1 agonist CH275 (Fig. 5L), suggesting that EC cells from the small intestine may upregulate surface expression of SSTR1 upon dissociation and loss of contact with neighboring epithelial cells.

EC cells potentiate visceral pain responses by sensitizing spinal afferent neurons that innervate the intestinal mucosa (9). Exogenous SSTR agonists have been shown to reduce visceral sensitivity, but these effects have been previously attributed to action either upon spinal afferents or more centrally in the pain pathway (35–38), so we were curious to know how SSTR signaling in EC cells might contribute to these effects. We first asked whether SSTRs are indeed expressed by relevant sensory neurons by performing single-cell RT-PCR of cholera toxin B-traced jejunal or colonic mucosal afferents from either the nodose or dorsal root ganglia, respectively. We found that mucosal afferents from both ganglia express multiple SSTRs, with spinal afferents to the colon expressing *Sstr1*, *Sstr4*, and less frequently, *Sstr2* (SI Appendix, Fig. S5). We also wondered whether *Sst*-expressing sensory neurons (39) innervate the gut and provide negative feedback to EC cells; *Sst* transcripts were found in few or no vagal or spinal mucosal afferents, suggesting that sensory neurons are not a major supplier of SST to EC cells. We then used ex vivo colon-pelvic nerve recordings to ask how SSTR-mediated inhibition of colonic EC cells might affect the sensitivity of mucosal afferents (Fig. 6A). Robust EC-cell driven sensitization of these neurons can be observed upon epithelial application of isovalerate, a microbiota-derived short-chain fatty acid (40) which directly activates EC cells but not mucosal afferents (Fig. 6B–D and H and SI Appendix, Fig. S6A and B) (2, 9). To more specifically target SSTRs on EC cells, we then exploited the poor epithelial permeability (41) of the SSTR2/3/5 agonist octreotide by applying it to a small area of the mucosal epithelium which was isolated from the rest of the recording chamber by a metal ring (Fig. 6A). Luminally applied octreotide did not diminish mucosal afferent responses across a wide range of mechanical stimulation intensities (Fig. 6E–G and I and SI Appendix, Fig. S6C and D), indicating that any fibers potentially expressing octreotide-sensitive SSTR2 receptors were not directly inhibited under our experimental regime. This observation is also consistent with the fact that baseline serotonin release

from EC cells is insufficient to activate mucosal afferents (6, 9). In contrast, octreotide robustly blocked the sensitizing effect of isovalerate (Fig. 6E–G, J, and K and SI Appendix, Fig. S6C and D), demonstrating that SSTR signaling in EC cells is sufficient to prevent their acute sensitization of mucosal afferents.

Discussion

Despite the diverse physiological functions that EC cells serve in the gut and their proposed role in GI disorders, our understanding of these and other enteroendocrine cells has lagged behind that of other cell types with sensory and secretory functions. This is in large part due to their anatomical location as an integral, yet sparsely dispersed constituent of the intestinal epithelium (1). In contrast, the mechanistic study of other sensory cells has been facilitated by their dense representation within anatomically discrete ganglia or specialized sensory structures (42).

Here, we describe a method for the large-scale in vitro visualization of individual EC cell activity within a physiologically relevant epithelial context. We use this technique to identify SST28 as a robust inhibitor of EC cells from both small intestine and colon via activation of multiple SSTR subtypes. The spatial and temporal resolution of these experiments allowed us to capture a subset of EC cells that exhibit an unexpected biphasic response to SST28, a behavior which was recapitulated by biosensor imaging of EC cells within the intact crypt-villus architecture of the gut. We subsequently used these insights to inform further interrogation of SSTR- G_i signaling in EC cells and found that this inhibitory pathway modulates voltage-gated calcium channels critical for serotonin release (2). Furthermore, we demonstrate that SSTR activation is sufficient to block EC cell-driven sensitization of sensory neurons that innervate the intestinal mucosa and relay nocifensive signals to the brain (9). Altogether, we show that in vitro biosensor-expressing organoid monolayers can be used as a starting point to enhance mechanistic understanding of EC cell pharmacology and physiology.

This approach has a number of advantages in assessing EC cell activity. For example, biosensor imaging is highly sensitive, temporally resolved, and scalable at low cost when compared to antibody-based measurement of serotonin release in supernatants from intestinal tissue or cultured cells. The small size (and consequently lower signal intensity) and sparsity of EC cells (whether cultured in 3D organoids, monolayers, or as isolated cells) constrain the scope of calcium imaging experiments. In contrast, g5-HT3.0-expressing epithelia surrounding each EC cell serve as a biological signal amplifier, permitting the use of low-magnification optics to monitor many cells at once (often >1,000 cells from up to 32 wells in our case). These advantages are shared by biosensor imaging of acutely isolated tissues, but such experiments are technically involved, limited by the number of recordings that can be obtained from a single animal (typically 1 to 4), and challenging to perform in other regions of the GI tract (such as the colon) due to differences in biosensor expression and/or tissue morphology. Other methods for measuring single-EC cell activity such as electrophysiology (2, 6, 15) or amperometry (43), while providing granular biological insight, are inherently low throughput. Furthermore, the relatively long duration of our biosensor recordings (up to 90 min) enables the quantification of even low-level, tonic EC activity, greatly facilitating the identification of inhibitory responses which, in our experience, can be more challenging to discern by other methods.

Cells within the intestinal epithelium are polarized and can preferentially target membrane proteins to either their apical or basolateral aspect (2, 15). As our subconfluent monolayers are

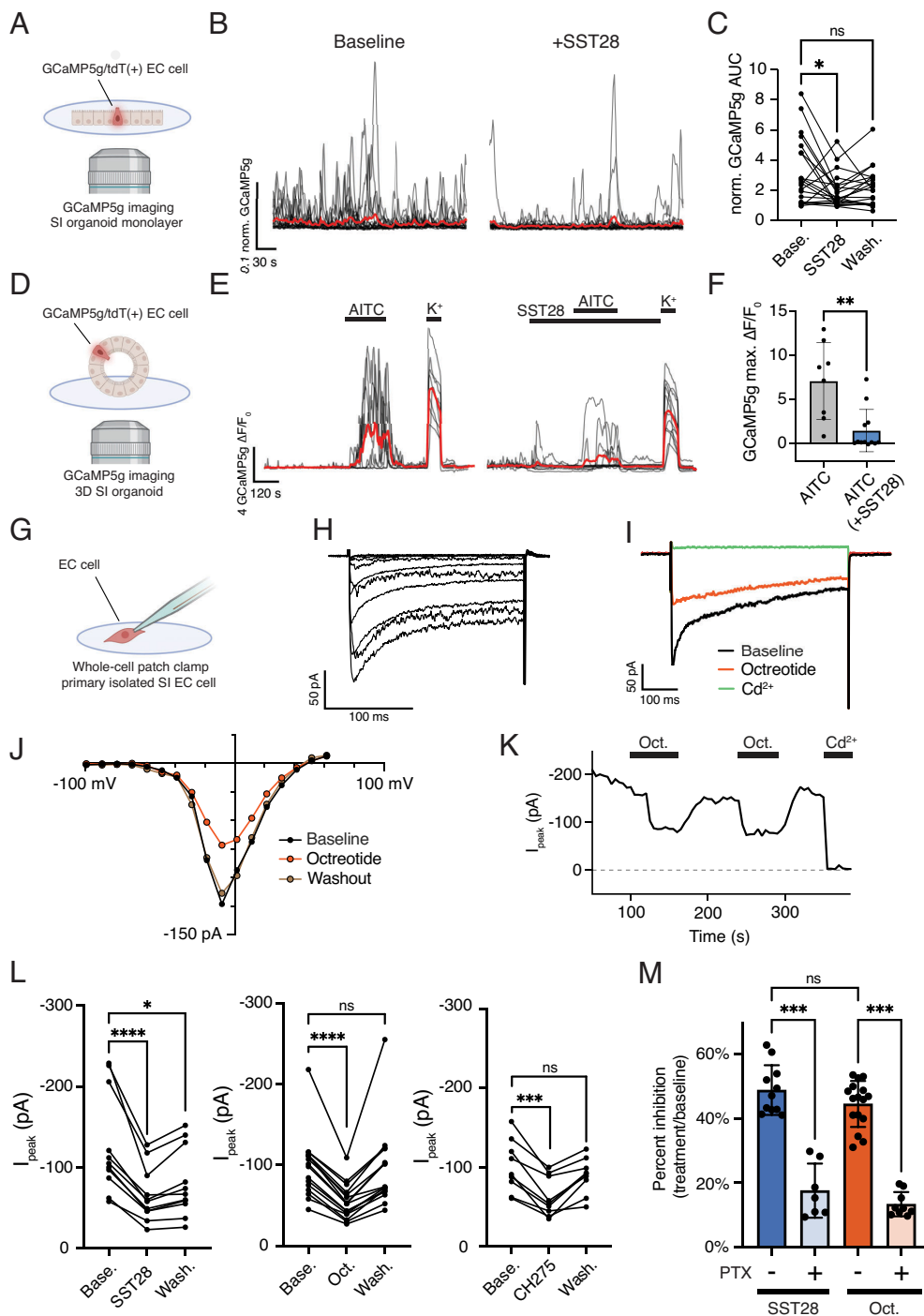


Fig. 5. SSTRs suppress EC cell activity via inhibition of voltage-gated calcium channels. (A) Ca^{2+} flux was visualized in EC cells expressing tdT and GCaMP5g within small intestinal organoid monolayers under constant perfusion. (B) Normalized GCaMP5g fluorescence traces showing tonic activity over 5 min periods before and during application of SST28 (300 nM). Average trace in red. (C) Effect of SST28 on normalized GCaMP5g area under the curve (AUC) from each period. Friedman test (Dunn's). Baseline vs. SST28, $P = 0.0216$. Baseline vs. washout, $P = 0.0615$ (not significant). $n = 21$ cells. (D) Ca^{2+} flux was visualized in EC cells expressing tdT and GCaMP5g within 3D organoids under constant perfusion. Organoids were removed from Matrigel matrix and adhered to Cell-Tak coated coverslips for imaging. (E) GCaMP5g fluorescence signals showing a reduction in AITC (10 μM)-evoked Ca^{2+} flux by SST28 (300 nM). High K^+ (75 mM) was added at the end of each recording. Average trace in red. (F) Effect of SST28 on maximum AITC-evoked GCaMP5g response. Mann-Whitney test, $P = 0.0015$. $n = 8$ to 12 cells. (G) Primary isolated small intestinal EC cells were identified by their expression of tdT and whole-cell patch clamp recording was performed to measure Ca_v channel activity. (H) Representative current traces showing depolarization-evoked Ca_v currents. For all Ca_v recordings, voltage-gated sodium and potassium channels were inhibited by N-methyl-D-glucamine and tetrodotoxin in the external solution and by Cs^+ in the internal solution. Ba^{2+} (10 mM) was used as the charge carrier to increase the conductance of Ca_v channels. Membrane potential was held at -118 mV and responses to 10 mV voltage steps from -83 mV to 27 mV are shown. (I) Representative current traces showing inhibition by octreotide (red). The general Ca_v blocker, cadmium (Cd^{2+} , green), was added at the end of the recording to verify that the recorded current was through Ca_v channels. Membrane potential was held at -118 mV and voltage steps to -8 mV were applied every 5 s. (J) Representative current-voltage plot showing peak inward current amplitude before (black), during (red), and after (brown) application of octreotide. Membrane potential was held at -118 mV and 10 mV voltage steps from -118 mV to 62 mV were applied during each period. (K) Representative current-time plot showing octreotide inhibition and washout. Cd^{2+} was added at the end of the recording. Membrane potential was held at -118 mV and voltage steps to -8 mV were applied every 5 s. (L) Peak inward current before, during, and after the application of SSTR agonists (all 300 nM). Membrane potential was held at -118 mV and voltage steps to -8 mV were applied every 5 s. Friedman tests (Dunn's). Baseline vs. SST28: $P < 0.0001$, baseline vs. washout (SST28): $P = 0.038$, baseline vs. octreotide: $P < 0.0001$, baseline vs. washout (octreotide): $P > 0.9999$ (not significant), Baseline vs. CH275: $P = 0.0005$, baseline vs. washout (CH275): $P = 0.6916$. $n = 9$ to 16 cells. (M) Effect of PTX (200 ng/mL) pretreatment on Ca_v inhibition by SST28 or octreotide (both 300 nM). Kruskal-Wallis test (Dunn's). SST28 vs. SST28 (PTX): $P = 0.0005$, octreotide vs. octreotide (PTX): $P = 0.0002$, SST28 vs. octreotide: $P > 0.9999$ (not significant). $n = 7$ to 16 cells. Error bars: SD. * $P \leq 0.05$. ** $P \leq 0.01$. *** $P \leq 0.001$. **** $P \leq 0.0001$.

cultured directly on the plate bottom, this method is likely to be more sensitive in detecting EC cell modulators that act upon apically expressed receptors. Alongside serotonin, EC cells also secrete other transmitters such as purines (6) and substance P (2). The workflow we describe here can be readily used in conjunction with other available biosensors (44–46) to measure the release of a wide range of signaling molecules from EC or other enteroendocrine cells, such as GLP-1, PYY, or, indeed, SST. While we derived g5-HT3.0-expressing organoids from transgenic mice, established gene editing protocols (47) can be applied to integrate

this or other biosensors into existing organoid lines, such as those derived from human tissues.

Local SST signaling mediates a diverse array of physiological processes throughout the body (26), such as hormone release in the pancreas (48), gastric acid secretion in the stomach (49), pruritoception (50), and sleep (51). Its short (1 to 3 min) biological half-life and relatively low (4 to 20 pM) circulating concentration (52) suggest that SST is predominantly a paracrine signal, acting within its tissue of origin (53). In the intestine, SST is expressed by enteroendocrine D cells (21) and a discrete

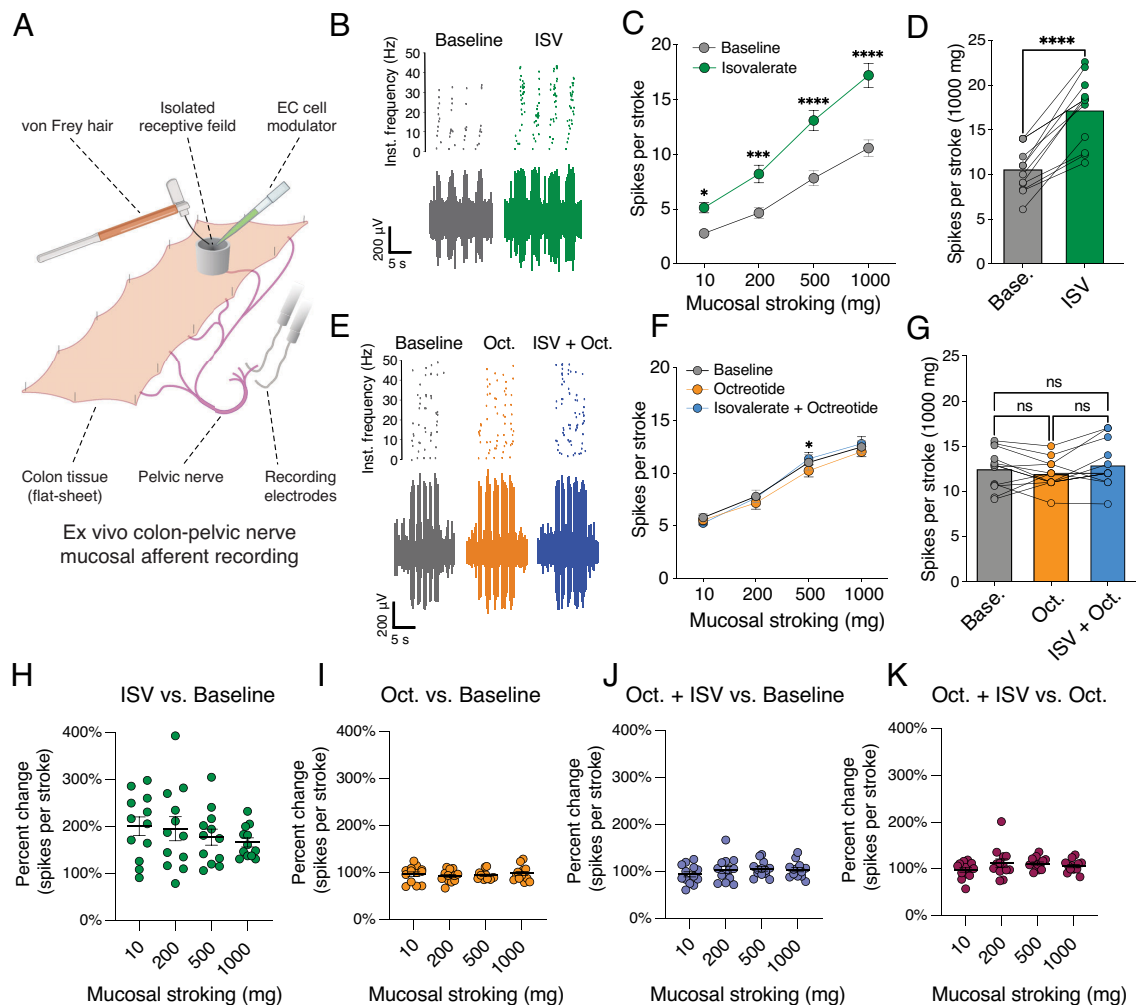


Fig. 6. Epithelial SST signaling blocks EC cell-driven mucosal afferent hypersensitivity. (A) Schematic of ex vivo “flat sheet” colon-pelvic nerve mucosal afferent recordings. (B) Representative action potential firing from single colonic mucosal afferent fibers elicited by a 1,000 mg von Frey hair stimulus stroked over the mucosal epithelium before and after application of isovalerate (ISV, 200 μ M). (C) Epithelial treatment with isovalerate enhances mechanical responses at all stroke weights. Two-way ANOVA (Šidák’s). 10 mg: $P = 0.0134$. 200 mg: $P = 0.001$. 500 mg: $P < 0.0001$. 1,000 mg: $P < 0.0001$. (D) Individual mucosal afferent responses to 1,000 mg strokes. Paired t test, $P < 0.0001$. (E) Representative action potential firing from single colonic mucosal afferent fibers elicited by a 1,000 mg von Frey hair stimulus stroked over the mucosal epithelium before or after application of octreotide (Oct., 300 nM) or octreotide and isovalerate. (F) Octreotide alone does not affect baseline mechanical responses, but does abrogate the sensitizing effect of isovalerate. Two-way ANOVA (Tukey’s). Octreotide vs. octreotide + isovalerate (500 mg stroke): $P = 0.0168$. All other comparisons: $P > 0.05$ (not significant). (G) Individual mucosal afferent responses to 1,000 mg strokes. Repeated measures one-way ANOVA (Tukey’s). All comparisons $P > 0.05$ (not significant). (H–K) Percent change in individual mucosal afferent firing after treatment with (H) isovalerate, (I) octreotide, or (J) isovalerate and octreotide (compared to baseline), and (K) isovalerate and octreotide (compared to octreotide). Error bars: SEM. $n =$ number of mucosal afferents, $N =$ number of mice. * $P \leq 0.05$. *** $P \leq 0.001$. **** $P \leq 0.0001$.

population of enteric neurons (54) yet physiological roles of SST signaling from these cells have yet to be rigorously defined (1, 55). Interestingly, SST agonists have been proposed to regulate intestinal peristalsis (56, 57), as well as reduce visceral sensitivity in both rodents and humans (35–38). Our findings suggest that direct modulation of EC cell activity may play a significant role in these effects. As such, defining the physiological circumstances under which SST-secreting cells communicate with EC cells in vivo is an important next goal that will likely require the use of genetic tools to specifically target these populations and/or visualize SST release and propagation within the intestine.

Beyond their role as primary sensors for noxious luminal stimuli (2, 5, 6), EC cells integrate a variety of aversive signals from other cells in the gut (2–4, 6). Negative regulation by SST highlights the role of these cells as critical nocifensive signaling hubs whose activity must be tightly controlled. Given the now well-validated role of EC cells in visceral hypersensitivity, it stands to reason that dysregulation of inhibitory mechanisms controlling their excitability may contribute to visceral pain and

GI dysmotility experienced by patients with IBS or other GI syndromes. If so, then SST-mediated signaling pathways may prove to be effective therapeutic targets for treating these disorders.

Materials and Methods

2D Organoid Monolayer Culture. 3D intestinal organoids were generated from either the jejunum or proximal colon of *Vil1^{Cre}; Rosa26^{g5-H2B}* mice as previously reported (58, 59) and briefly described in *SI Appendix, SI Materials and Methods*. 2D organoid monolayers were generated using a modified protocol (60). Six days after passage, organoid culture media were refreshed. The following day, organoids were removed from Matrigel (Corning), washed once in 10 mL basal media (advanced Dulbecco’s Modified Eagle Medium [DMEM]/F12 with penicillin/streptomycin, 10 mM 4-(2-hydroxyethyl)-1-piperazineethanesulfonic acid [HEPES], and Glutamax [Thermo Fisher Scientific]), broken up into crypts/fragments with a 1,000 μ L pipette, and then washed twice in 10 mL basal media to remove cell debris and residual Matrigel. Organoid fragments were resuspended in TrypLE Express (Thermo Fisher Scientific) with 10 μ M Y-27632 (Sigma) and triturated with a 1,000 μ L pipette for 2 to 3 min to generate a mixture of single cells and

small clumps. This suspension was washed in 10 mL basal media, resuspended in organoid culture media with 10 μ M Y-27632 and 3 μ M CHIR-99021, and seeded onto 384-well imaging plates (Corning) precoated with 5% Matrigel solution. After 16 h, monolayers were washed twice with basal media and cultured in fresh organoid culture media.

g5-HT3.0 Imaging of Organoid Monolayers. Small intestine and colon organoid monolayers were imaged 2 and 4 d after seeding, respectively. For PTX experiments, 200 ng/mL PTX (Tocris) or vehicle was added to each well 24 h prior to imaging. For YM254890 experiments, 1 μ M YM254890 (Tocris) or vehicle was added to each well 60 min prior to imaging. On the day of imaging, other reagents were prepared at 4 \times final concentration in BSA/Ringer's solution (140 mM NaCl, 5 mM KCl, 2 mM CaCl₂, 2 mM MgCl₂, 10 mM D-glucose, and 10 mM HEPES-Na, 0.01% bovine serum albumen [BSA, A4161, Sigma], pH 7.4). At time of imaging, monolayers were washed once with Dulbecco's phosphate buffered saline with Ca²⁺/Mg²⁺ (Thermo Fisher Scientific) containing 0.2% BSA, twice with BSA/Ringer's solution, and then imaged in 80 μ L BSA/Ringer's solution using an Image Express Confocal HT.ai microscope (Molecular Devices) equipped with a Zyla 4.5 camera (Andor), 475 nm LDI laser (89 North), and MetaXpress software (Molecular Devices). g5-HT3.0 biosensor fluorescence from each well was recorded using widefield time series imaging at room temperature with an exposure time of 200 ms, laser power of 15%, and acquisition interval of 30 s. In each experiment, baseline EC cell activity was recorded for at least 20 min prior to reagent application. Reagents were applied with a 50 μ L multichannel pipette by first removing 20 μ L of recording media from each well and then replacing it with 20 μ L of prepared 4 \times stock. At the end of every recording, thapsigargin (4 μ M) was applied to facilitate identification of EC cells and then serotonin (20 μ M) was applied to fully activate g5-HT3.0 for normalization. Note that sensitive g5-HT3.0 imaging requires a recording solution with minimal autofluorescence, precluding the use of reagents required for sustained organoid culture. Experiments were limited to less than 90 min to avoid gradual cell detachment which could be observed over longer timeframes.

Analysis of g5-HT3.0 Monolayer Imaging Data. Time series imaging data were analyzed using Fiji software v2.14 (NIH). Image stacks for each well were motion-corrected with moco (61) and then circular regions of interest (ROI, dia. 30 px., 103.8 μ m) were drawn centered around each EC cell. Any EC cells with overlapping ROIs were excluded from subsequent analysis. In each well, an additional ROI was drawn around an exposed area of the plate bottom for later background subtraction. Mean fluorescence intensity over time was measured for each ROI and subsequently analyzed in R v4.3.2 (62) with biostatistical consultation from the University of California, San Francisco Clinical and Translational Science Institute. Data from each EC cell were background-subtracted and then normalized to the individual pretreatment baseline intensity and the maximum intensity elicited by exogenous serotonin at the end of each recording. To determine drug effects, the normalized g5-HT3.0 signals were used to calculate relative maximum and volatility (as described in *Results*) between 10-min periods before and after treatment. EC cells were excluded from further analysis if normalized g5-HT3.0 intensity was at any point higher than 0.4 during the baseline period or lower than -0.7 or higher than 0.9 during

either analysis period. To determine drug pretreatment effects on baseline activity, log-transformed signal maximum and volatility in the baseline period were used for comparison between groups. Statistical analysis was performed using a Generalized Estimating Equation model with an exchangeable correlation structure and robust SE to account for the clustering of cells within wells. Outlier detection and model assumptions were tested using Quantile-Quantile plots and D'Agostino tests (63). EC cells exhibiting acute activation by SST28 were systematically identified by comparing maximum normalized g5-HT3.0 intensity across a total of three time periods: P1 (10-0 min before treatment), P2 (0 to 2.5 min after treatment), P3 (10 to 20 min after treatment). Identification criteria were P2/P1 > 2, P2 - P1 > 0.09, and P2 - P3 > 0.07. Percent responder data were analyzed using Fisher's Exact Test. All *P* values were adjusted for multiple post hoc comparisons (Bonferroni).

Other Materials and Methods. All other materials and methods are presented in *SI Appendix, SI Materials and Methods*.

Data, Materials, and Software Availability. RNA sequencing data are available under Gene Expression Omnibus ID [GSE291832](https://www.ncbi.nlm.nih.gov/geo/query/acc.cgi?acc=GSE291832). Custom R code used to analyze g5-HT3.0 monolayer imaging data has been deposited on GitHub (64). Reagents used here will be shared upon reasonable request to the corresponding author. All other study data are provided in the article or *SI Appendix*.

ACKNOWLEDGMENTS. We thank Ms. Jeannie Poblete for her technical support. We thank Dr. James Bayrer, Dr. Holly Ingraham, and all members of the Julius lab for discussion. We thank Dr. Joni Nikkanen for assistance with bulk RNA sequencing analysis. We thank Dr. Karla Lindquist for biostatistical consultation. We appreciate the support from staff in UCSF's core facilities, including the Innovation Core at the Weill Institute for Neurosciences (Dr. Caroline Mrejen), the Center for Advanced Light Microscopy (Dr. So Yeon Kim and Dr. Kari Herrington), and the Laboratory for Cell Analysis (Dr. Sarah Elmes). This work was supported by NIH grants NS105038, and DK135714 to D.J.; National Health and Medical Research Council (NHMRC) of Australia Investigator Leadership Grant (APP2008727) to S.M.B.; BRAIN Initiative grants 1U01NS113358 and 1U01NS120824, the National Natural Science Foundation of China grant 31925017, the New Cornerstone Science Foundation through the New Cornerstone Investigator Program and the XPLOER PRIZE to Y.L.; NHMRC Ideas Grant APP2029332 to J.C.; Australian Research Council Discovery Projects DP180101395 and DP22010126 to A.M.H.; Damon Runyon Cancer Research Foundation Fellowship (DRG-[2387-30]) to K.K.T.; and NIH institutional training grant (5T32GM139786-02) to N.D.R. Graphical schemes were created in BioRender [BioRender. N.D.R. (2025) <https://BioRender.com/k58j939j>].

Author affiliations: ^aDepartment of Physiology, University of California, San Francisco, CA 94158; ^bTetrad Graduate Program, Graduate Division, University of California, San Francisco, CA 94158; ^cVisceral Pain Research Group, Hopwood Centre for Neurobiology, Lifelong Health Theme, South Australian Health and Medical Research Institute, Adelaide, SA 5000, Australia; ^dFaculty of Health and Medical Sciences, University of Adelaide, Adelaide, SA 5000, Australia; ^eState Key Laboratory of Membrane Biology, New Cornerstone Science Laboratory, School of Life Sciences, Peking University, Beijing 100871, China; and ^fInternational Data Group / McGovern Institute for Brain Research at Peking University, Beijing 100871, China

1. F. M. Gribble, F. Reimann, Enteroreceptors: Chemosensors in the intestinal epithelium. *Annu. Rev. Physiol.* **78**, 277-299 (2016).
2. N. W. Bellono *et al.*, Enterochromaffin cells are gut chemosensors that couple to sensory neural pathways. *Cell* **170**, 185-198.e16 (2017).
3. M. L. Lund *et al.*, Enterochromaffin 5-HT cells—A major target for GLP-1 and gut microbial metabolites. *Mol. Metab.* **11**, 70-83 (2018).
4. Z. Chen *et al.*, Interleukin-33 promotes serotonin release from enterochromaffin cells for intestinal homeostasis. *Immunity* **54**, 151-163.e6 (2020).
5. C. Alcaino *et al.*, A population of gut epithelial enterochromaffin cells is mechanosensitive and requires Piezo2 to convert force into serotonin release. *Proc. Natl. Acad. Sci. U.S.A.* **115**, E7632-E7641 (2018).
6. K. K. Touhara *et al.*, Topological segregation of stress sensors along the gut crypt-villus axis. *Nature* **640**, 732-742 (2025).
7. A. J. Treichel *et al.*, Specialized mechanosensory epithelial cells in mouse gut intrinsic tactile sensitivity. *Gastroenterology* **162**, 535-547.e13 (2022).
8. Z. Xie *et al.*, The gut-to-brain axis for toxin-induced defensive responses. *Cell* **185**, 4298-4316.e21 (2022).
9. J. R. Bayrer *et al.*, Gut enterochromaffin cells drive visceral pain and anxiety. *Nature* **616**, 137-142 (2023).
10. G. M. Mawe, J. M. Hoffman, Serotonin signalling in the gut—functions, dysfunctions and therapeutic targets. *Nat. Rev. Gastroenterol. Hepatol.* **10**, 473-486 (2013).
11. D. M. Brenner, G. S. Sayuk, Current US food and drug administration-approved pharmacologic therapies for the treatment of irritable bowel syndrome with diarrhea. *Adv. Ther.* **37**, 83-96 (2020).
12. K. Sjölund, G. Sandén, R. Håkanson, F. Sundler, Endocrine cells in human intestine: An immunocytochemical study. *Gastroenterology* **85**, 1120-1130 (1983).
13. E. J. Forsberg, R. J. Miller, Regulation of serotonin release from rabbit intestinal enterochromaffin cells. *J. Pharmacol. Exp. Ther.* **227**, 755-766 (1983).
14. M. Kidd, I. M. Modlin, G. N. Eick, M. C. Champaneria, Isolation, functional characterization, and transcriptome of *Mastomys* ileal enterochromaffin cells. *Am. J. Physiol. Gastrointest. Liver Physiol.* **291**, G778-G791 (2006).
15. P. R. Streve *et al.*, Sodium channel NaV1.3 is important for enterochromaffin cell excitability and serotonin release. *Sci. Rep.* **7**, 15650 (2017).
16. B. L. Sabatini, L. Tian, Imaging neurotransmitter and neuromodulator dynamics in vivo with genetically encoded indicators. *Neuron* **108**, 17-32 (2020).
17. Z. Wu, D. Lin, Y. Li, Pushing the frontiers: Tools for monitoring neurotransmitters and neuromodulators. *Nat. Rev. Neurosci.* **23**, 257-274 (2022).
18. F. Deng *et al.*, Improved green and red GRAB sensors for monitoring spatiotemporal serotonin release in vivo. *Nat. Methods* **21**, 692-702 (2024).

19. C. A. Thorne *et al.*, Enteroid monolayers reveal an autonomous WNT and BMP circuit controlling intestinal epithelial growth and organization. *Dev. Cell* **44**, 624–633.e4 (2018).
20. S.-E. Jordt *et al.*, Mustard oils and cannabinoids excite sensory nerve fibres through the TRP channel ANKTM1. *Nature* **427**, 260–265 (2004).
21. M. Ravazzola, R. Benoit, N. Ling, R. Guillemain, L. Orci, Immunocytochemical localization of prosomatostatin fragments in maturing and mature secretory granules of pancreatic and gastrointestinal D cells. *Proc. Natl. Acad. Sci. U.S.A.* **80**, 215–218 (1983).
22. Y. C. Patel, T. Wheatley, C. Ning, Multiple forms of immunoreactive somatostatin: comparison of distribution in neural and nonneural tissues and portal plasma of the rat. *Endocrinology* **109**, 1943–1949 (1981).
23. Y. C. Patel, W. O'Neil, Peptides derived from cleavage of prosomatostatin at carboxyl- and amino-terminal segments. Characterization of tissue and secreted forms in the rat. *J. Biol. Chem.* **263**, 745–751 (1988).
24. B. H. Francis, D. G. Baskin, D. R. Saunders, J. W. Ensink, Distribution of somatostatin-14 and somatostatin-28 gastrointestinal-pancreatic cells of rats and humans. *Gastroenterology* **99**, 1283–1291 (1990).
25. D. F. Trent, G. C. Weir, Heterogeneity of somatostatin-like peptides in rat brain, pancreas, and gastrointestinal tract. *Endocrinology* **108**, 2033–2038 (1981).
26. T. Günther *et al.*, International union of basic and clinical pharmacology. CV. Somatostatin receptors: Structure, function, ligands, and new nomenclature. *Pharmacol. Rev.* **70**, 763–835 (2018).
27. S. Chen, X. Teng, S. Zheng, Molecular basis for the selective G protein signaling of somatostatin receptors. *Nat. Chem. Biol.* **19**, 133–140 (2023).
28. J. K. Kim *et al.*, PDZ domain-containing 1 (PDZK1) protein regulates phospholipase C- β 3 (PLC- β 3)-specific activation of somatostatin by forming a ternary complex with PLC- β 3 and somatostatin receptors. *J. Biol. Chem.* **287**, 21012–21024 (2012).
29. E. M. Pfeil *et al.*, Heterotrimeric G protein subunit G α q is a master switch for G β γ -mediated calcium mobilization by Gi-coupled GPCRs. *Mol. Cell* **80**, 940–954.e6 (2020).
30. Y. C. Patel, C. B. Srikant, Subtype selectivity of peptide analogs for all five cloned human somatostatin receptors (hsstr 1–5). *Endocrinology* **135**, 2814–2817 (1994).
31. Y. Song *et al.*, Stratification of enterochromaffin cells by single-cell expression analysis. *Elife* **12**, RP90596 (2023).
32. J. Beumer *et al.*, Description and functional validation of human enteroendocrine cell sensors. *Science* **386**, 341–348 (2024).
33. J. Beumer *et al.*, High-resolution mRNA and secretome atlas of human enteroendocrine cells. *Cell* **181**, 1291–1306.e19 (2020).
34. K. M. Betke, C. A. Wells, H. E. Hamm, GPCR mediated regulation of synaptic transmission. *Prog. Neurobiol.* **96**, 304–321 (2012).
35. X. Su, M. Burton, G. Gebhart, Effects of octreotide on responses to colorectal distension in the rat. *Gut* **48**, 676–682 (2001).
36. I. Schwetz *et al.*, Anti-hyperalgesic effect of octreotide in patients with irritable bowel syndrome. *Aliment Pharmacol. Ther.* **19**, 123–131 (2004).
37. A. Mulak *et al.*, Selective agonists of somatostatin receptor subtype 1 or 2 injected peripherally induce antihyperalgesic effect in two models of visceral hypersensitivity in mice. *Peptides* **63**, 71–80 (2015).
38. M. Bradette *et al.*, Octreotide increases thresholds of colonic visceral perception in IBS patients without modifying muscle tone. *Dig. Dis. Sci.* **39**, 1171–1178 (1994).
39. L. Qi *et al.*, A mouse DRG genetic toolkit reveals morphological and physiological diversity of somatosensory neuron subtypes. *Cell* **187**, 1508–1526.e16 (2024).
40. C.-J. Guo *et al.*, Depletion of microbiome-derived molecules in the host using Clostridium genetics. *Science* **366**, eaav1282 (2019).
41. G. Fricker *et al.*, Permeation enhancement of octreotide by specific bile salts in rats and human subjects: In vitro, in vivo correlations. *Br. J. Pharmacol.* **117**, 217–223 (1996).
42. C. U. M. Smith, *Biology of Sensory Systems* (John Wiley & Sons, ed. 2, 2008).
43. R. Raghupathi *et al.*, Identification of unique release kinetics of serotonin from guinea-pig and human enterochromaffin cells. *J. Physiol.* **591**, 5959–5975 (2013).
44. H. Wang *et al.*, A tool kit of highly selective and sensitive genetically encoded neuropeptide sensors. *Science* **382**, eaq8173 (2023).
45. Z. Wu *et al.*, A sensitive GRAB sensor for detecting extracellular ATP in vitro and in vivo. *Neuron* **110**, 770–782.e5 (2022).
46. L. Duffet *et al.*, Optical tools for visualizing and controlling human GLP-1 receptor activation with high spatiotemporal resolution. *Elife* **12**, RP86628 (2023).
47. M. H. Geurts, H. Clevers, CRISPR engineering in organoids for gene repair and disease modelling. *Nat. Rev. Bioeng.* **1**, 32–45 (2023).
48. P. Rorsman, M. O. Huisin, The somatostatin-secreting pancreatic δ -cell in health and disease. *Nat. Rev. Endocrinol.* **14**, 404–414 (2018).
49. M. L. Schubert, D. A. Peura, Control of gastric acid secretion in health and disease. *Gastroenterology* **134**, 1842–1860 (2008).
50. J. Huang *et al.*, Circuit dissection of the role of somatostatin in itch and pain. *Nat. Neurosci.* **21**, 707–716 (2018).
51. K. Tossell *et al.*, Somatostatin neurons in prefrontal cortex initiate sleep-preparatory behavior and sleep via the preoptic and lateral hypothalamus. *Nat. Neurosci.* **26**, 1805–1819 (2023).
52. U. Rai, T. R. Thrimawithana, C. Valery, S. A. Young, Therapeutic uses of somatostatin and its analogues: Current view and potential applications. *Pharmacol. Ther.* **152**, 98–110 (2015).
53. B. K. Mani, J. M. Zigman, A strong stomach for somatostatin. *Endocrinology* **156**, 3876–3879 (2015).
54. E. Drokhyansky *et al.*, The human and mouse enteric nervous system at single-cell resolution. *Cell* **182**, 1606–1622.e23 (2020).
55. S. Schneider, C. M. Wright, R. O. Heuckeroth, Unexpected roles for the second brain: Enteric nervous system as master regulator of bowel function. *Annu. Rev. Physiol.* **81**, 235–259 (2019).
56. F. Abdu, G. A. Hicks, G. Hennig, J. P. Allen, D. Grundy, Somatostatin sst2 receptors inhibit peristalsis in the rat and mouse jejunum. *Am. J. Physiol. Gastrointest. Liver Physiol.* **282**, G624–G633 (2002).
57. T. Takeda, K. Taniyama, S. Baba, C. Tanaka, Putative mechanisms involved in excitatory and inhibitory effects of somatostatin on intestinal motility. *Am. J. Physiol.* **257**, G532–538 (1989).
58. H. Miyoshi, T. S. Stappenbeck, In vitro expansion and genetic modification of gastrointestinal stem cells in spheroid culture. *Nat. Protoc.* **8**, 2471–2482 (2013).
59. T. Sato *et al.*, Single Lgr5 stem cells build crypt-villus structures in vitro without a mesenchymal niche. *Nature* **459**, 262–5 (2009).
60. L. E. Sanman *et al.*, "Generation and quantitative imaging of enteroid monolayers" in *Intestinal Stem Cells*, P. Ordóñez-Morán, Ed. (*Methods in Molecular Biology*, Springer US, 2020), pp. 99–113.
61. A. Dubbs, J. Guevara, R. Yuste, moco: Fast motion correction for calcium imaging. *Front. Neuroinform.* **10**, 6 (2016).
62. R Core Team, R: A Language and Environment for Statistical Computing (v4.3.2, R Foundation for Statistical Computing, Vienna, Austria, 2025). <https://www.R-project.org/>. Accessed 31 October 2023.
63. R. B. D'agostino, Transformation to normality of the null distribution of g1. *Biometrika* **57**, 679–681 (1970).
64. N. D. Rossen, monolayer_analysis. (2025). https://github.com/rossenn/monolayer_analysis. Deposited 12 March 2025.